Practical Implementation of a Reset Controller to Improve Performance of an Industrial Motion Stage

Caporale, Daniel; van Eijk, Luke F.; Karbasizadeh, Nima; Beer, Stijn; Kostic, Dragan; HosseinNia, S. Hassan

DOI
10.1109/TCST.2024.3374155

Publication date
2024

Document Version
Final published version

Published in
IEEE Transactions on Control Systems Technology

Citation (APA)
Caporale, D., van Eijk, L. F., Karbasizadeh, N., Beer, S., Kostic, D., & HosseinNia, S. H. (2024). Practical Implementation of a Reset Controller to Improve Performance of an Industrial Motion Stage. *IEEE Transactions on Control Systems Technology*, *32*(4), 1451-1462. https://doi.org/10.1109/TCST.2024.3374155

Practical Implementation of a Reset Controller to Improve Performance of an Industrial Motion Stage

Daniel Caporale, Luke F. van Eijk, Nima Karbasizadeh, *Member, IEEE*, Stijn Beer, Dragan Kostić, and S. Hassan HosseinNia, *Senior Member, IEEE*

***Abstract*— In this work, the proportional Clegg integrator (PCI), a resetting proportional-integrator (PI) element, is studied with the aim of improving the performance of an industrial motion stage currently controlled by a linear controller. A novel parallel continuous reset (CR) architecture, based on the PI, is presented, along with frequency-based tuning guidelines, similar to linear time-invariant (LTI) loopshaping techniques. Open-loop higher order sinusoidal input describing functions (HOSIDFs) and pseudo-sensitivities computed through analytically derived approximate closed-loop HOSIDFs were effectively applied to predict steady-state performance. The experimental results, obtained on a wire bonding machine, confirmed that resonance-induced vibrations of the machine's base frame can be suppressed more effectively by adopting a PCI-PID controller compared to the currently used linear controller. The novel structure does not only reduce unwanted excitation of higher order harmonics of the base frame resonance, such as the series CR architecture recently introduced in literature, but also avoids amplification of noise when implemented in practice. With the novel parallel structure, a significant (32%) decrease in the root mean square (rms) of the settling error could be achieved when compared to the linear controller currently used and the series CR reset structure.**

***Index Terms*— Clegg integrator, higher order sinusoidal input describing function (HOSIDF), precision motion control, reset control systems.**

Manuscript received 21 January 2023; revised 15 August 2023, 22 December 2023, and 24 December 2023; accepted 11 February 2024. Date of publication 19 March 2024; date of current version 25 June 2024. This work was supported in part by ASMPT and in part by the Nederlandse Organisatie voor Wetenschappelijk Onderzoek (NWO), through the Open Technology Program (OTP) of the Applied and Engineering Sciences (AES) Project, under Grant 16335. *(Luke F. van Eijk and Nima Karbasizadeh contributed equally to this work.)* Recommended by Associate Editor J. T. Gravdahl. *(Corresponding author: S. Hassan HosseinNia.)*

Daniel Caporale and Nima Karbasizadeh were with the Department of Precision and Microsystems Engineering, Delft University of Technology, 2628 CB Delft, The Netherlands. They are now with ASML, 5504 DR Veldhoven, The Netherlands (e-mail: daniel.caporale@asml.com; nima.karbasizadeh.esfahani@asml.com).

Luke F. van Eijk is with the Department of Precision and Microsystems Engineering, Delft University of Technology, 2628 CB Delft, The Netherlands, and also with ASMPT, 6641 TL Beuningen, The Netherlands (e-mail: luke.van.eijk@asmpt.com).

Stijn Beer was with ASMPT, 6641 TL Beuningen, The Netherlands. He is now with ASML, 5504 DR Veldhoven, The Netherlands (e-mail: stijn.beer@asml.com).

Dragan Kostić is with ASMPT, 6641 TL Beuningen, The Netherlands (e-mail: dragan.kostic@asmpt.com).

S. Hassan HosseinNia is with the Department of Precision and Microsystems Engineering, Delft University of Technology, 2628 CB Delft, The Netherlands (e-mail: s.h.hosseinniakani@tudelft.nl).

Digital Object Identifier 10.1109/TCST.2024.3374155

I. Introduction

LINEAR time-invariant (LTI) control is indisputably the most popular choice for motion control strategies, with the overwhelming majority of industry relying on it [1]. The success of LTI control can be attributed to the simplicity it offers regarding the controller design process. This strategy allows for the use of classical control theory, which offers frequency-domain analysis tools to predict the steady-state performance, as well as determine stability and robustness of feedback systems. All of these analysistools can be deployed based solely on a nonparametric plant model, i.e., a frequency response function (FRF). Often, these tools are utilized in industry to shape the open- and closed-loop transfer functions to obtain the desired controller characteristics, what is often referred to as loopshaping [2]. Nevertheless, LTI control suffers from inherent limitations, such as the "waterbed effect" [3] and "Bode's gain–phase relationship" [4]. Therefore, employing such controllers creates a tradeoff between, e.g., rise time, tracking precision, noise suppression, and robustness. Improving one characteristic requires to worsen at least one of the other characteristics as a consequence. For this reason, for the last few decades, nonlinear control has been given great consideration in literature. Analytical proof, which shows that certain inherent limitations of LTI control can be overcome, is available for three nonlinear control elements; the hybrid integrator-gain system (HIGS) [5], reset control [6], and variable gain control (VGC) [7]. Nevertheless, adoption of nonlinear control techniques in industry is still scarce [1]. One of the main contributing factors is that getting a reliable indication of the system's steady-state performance in the frequency domain is for most techniques not possible, thus preventing the use of loopshaping techniques [8]. In VGC, the gain of the controller is dependent on the input amplitude, allowing to have a steeper magnitude slope in the open-loop FRF at low and high frequencies, respectively, due to the difference in amplitude between low- and high-frequency disturbances/noise. This technique allows for better suppression of low-frequent disturbances and high-frequent noise [9]. However, since the frequency response of such a filter is also dependent on the amplitude of the input [10], this control technique is unsuitable for systems whose reference is unknown a priori, thus for many industrial applications. The same issue does not occur

for HIGS and reset control since their nonlinearity is not amplitude-dependent. Among the two, reset control offers better frequency-based steady-state performance prediction methods, including closed-loop methods [10], [11], which are lacking for HIGS-based systems [12]. Numerous other (more popular) nonlinear control techniques exist, such as adaptive sliding mode control [13]. However, for these techniques, there are no intuitive methods available to design a controller that outperforms a well-designed LTI controller in an industrial setting, solely based on a nonparametric model of the plant, e.g., using frequency-domain analysis tools. With this work, the authors hope to get one step closer toward this goal for reset control in specific.

Reset control appeared for the first time in literature more than 60 years ago [14]. However, only four decades later, the field of reset control has been given enough attention to be considered a potentially reliable alternative to linear control [15]. Recent literature demonstrated that frequency-domain-based steady-state performance prediction and stability analysis methods exist for some particular reset control structures [11]. These methods make it possible to design and analyze such nonlinear controllers in a similar way as linear controllers while overcoming the inherent limitations of their linear counterparts. A considerable part of literature works are focused on the "constant in gain-lead in phase" (CgLp) element [16], [17], [18]. Nevertheless, this reset element is complex to tune and simplicity is of high importance in industry.

A different structure, known as the proportional Clegg integrator (PCI), allows a larger low-frequency open-loop gain compared to an equivalent LTI proportional-integrator (PI) system, for the same phase margin, based on a sinusoidal input describing function (SIDF) analysis. This additional gain leads to improved disturbance suppression when paired with an LTI PID, thus potentially improving the tracking performance of the system. Even though the PCI has a simpler structure than the CgLp element, it has been studied in literature for such purpose only once. In [19], a PCI-PID system was compared to a PI-PID system for reference tracking, with the former one not being able to outperform its linear counterpart. However, after [19], new steady-state performance analysis tools were developed. In addition, Karbasizadeh and HosseinNia [20] recently demonstrated that the performance of a reset element can be potentially further improved when used in a continuous reset (CR) architecture, capable of reducing the nonlinearity of the reset element over a broad frequency band.

The aim of this article is to study the viability of a PCI-PID controller, within the CR framework, for increasing the performance of an industrial motion stage. We demonstrate that while the CR architecture as presented in [20] achieves good results in simulations when applied in practice, a detrimental issue arises: measurement noise is amplified, leading to poor performance. Therefore, a novel parallel CR structure is implemented to ensure the low-frequency disturbance suppression of the PCI and to reduce broadband nonlinearities of the CR element. State-of-the-art frequency-domain analysis tools are used to analyze the controllers. The findings are experimentally validated on the motion stage of an industrial wire bonder, a machine that creates interconnections between chips and their packaging.

Section II includes the necessary background theory in terms of reset control. In Section III, the PCI-PID structure will be introduced. The advantages and drawbacks of the series CR architecture are also presented. A novel parallel CR structure is presented in Section IV, along with tuning guidelines. In Section V, a discrete-time implementation of the reset controller is proposed. This implementation is utilized in Section VI, where experimental results on a wirebonding machine are discussed. Finally, conclusions and suggestions for future work are given in Section VII.

II. Preliminaries

A. Definition of Reset Element

In this article, the definition from [11], given as

$$\mathcal{R} = \begin{cases} \dot{x}_r(t) = A_r x_r(t) + B_r e_r(t), & \text{if } \big(x_r(t), e_r(t)\big) \notin \mathcal{M} \\ x_r^+(t) = A_\rho x_r(t), & \text{if } \big(x_r(t), e_r(t)\big) \in \mathcal{M} \\ u_r(t) = C_r x_r(t) + D_r e_r(t) \end{cases} \tag{1}$$

is used to describe a single-input single-output (SISO) reset system $\mathcal{R}$. The first and last lines of (1) describe a standard LTI system in state space, where $A_r \in \mathbb{R}^{n_r \times n_r}$, $B_r \in \mathbb{R}^{n_r \times 1}$, $C_r \in \mathbb{R}^{1 \times n_r}$, and $D_r \in \mathbb{R}$ are the base linear system (BLS) matrices, $x_r(t) \in \mathbb{R}^{n_r \times 1}$ is the reset element's state vector with $n_r \in \mathbb{N}$ number of states, $e_r(t) \in \mathbb{R}$ is its input, $u_r(t) \in \mathbb{R}$ is its output, and $t \in \mathbb{R}^+$ indicates time. For the sake of brevity, the dependency on t will be omitted henceforward. The LTI system description holds true whenever (x_r, e_r) is not part of the reset surface $\mathcal{M}$. If, however, (x_r, e_r) is part of $\mathcal{M}$, the after-reset state at the reset time instant $x_r^+ = \lim_{y \to t+0} x_r(y)$ is determined by the reset matrix $A_\rho = \text{diag}(\gamma_1, \ldots, \gamma_{n_r})$, with $|\gamma_i| \leq 1 \, \forall i \in \mathbb{N}$. If $A_\rho = I^{n_r \times n_r}$, resets do not affect the system, which thus behaves like its BLS, defined as

$$R(s) = C_r(sI - A_r)^{-1}B_r + D_r \tag{2}$$

with $s \in \mathbb{C}$ being the Laplace variable.

In this work, we define the reset surface as

$$\mathcal{M} := \{e_r = 0 \wedge (I - A_\rho)x_r \neq 0\}. \tag{3}$$

Namely, for this reset condition, a prediction method has been developed in [10], which can fully accurately describe the open-loop steady-state performance using higher order SIDFs (HOSIDFs), based solely on an FRF of the plant. Furthermore, this method has been extended to also provide an approximation of the closed-loop steady-state performance [10], which we will exploit later in this work (more detail in Section II-C). Another popular reset condition is the one where resets occur when the input and output have opposite sign [21]. However, no similar HOSIDF method is available for this condition. Open-loop performance prediction based on HOSIDFs has been investigated for one other reset condition, which initiates resets based on a time-dependent

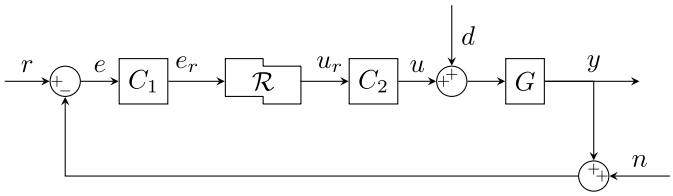

Fig. 1. Reset control feedback system architecture (adapted from [11]).

trigger signal [22]. However, no closed-loop performance prediction method based on HOSIDFs has been developed for this type of reset condition.

B. Control System Architecture

In [11], the closed-loop reset system architecture depicted in Fig. 1 was presented. C_1 and C_2 are SISO LTI filters, G is the plant, $r \in \mathbb{R}$ is the reference, $u \in \mathbb{R}$ is defined as the controller output, $d \in \mathbb{R}$ is the disturbance, $n \in \mathbb{R}$ is the sensor noise, $y \in \mathbb{R}$ is the true output, $y^* = y + n$ is the measured output, $e = r - y^*$ is the error, and $v = u + d$ is the plant input.

C. Predictive Performance

The steady-state input–output relationship of an LTI system can be straightforwardly computed based on its transfer function or FRF. As an example, consider SISO LTI system C_1 subject to a sinusoidal input

$$e(t) = \hat{e}\sin(\omega t + \varphi_e) \tag{4}$$

with input frequency $\omega \in \mathbb{R}^+$, amplitude $\hat{e} \in \mathbb{R}^+$, and phase $\varphi_e \in \mathbb{R}$. Then, this element's steady-state output signal is given by

$$e_r(t) = |C_1(j\omega)|\hat{e}\sin\left(\omega t + \varphi_e + \angle C_1(j\omega)\right) \tag{5}$$

where $C_1(j\omega)$ is the FRF of the respective LTI system. For reset controllers as in (1), the output signal is generally not a pure sinusoid when subject to a sinusoidal input

$$e_r(t) = \hat{e}_r\sin(\omega t + \varphi_{e_r}) \tag{6}$$

with input amplitude $\hat{e}_r \in \mathbb{R}^+$ and phase $\varphi_{e_r} \in \mathbb{R}$. However, since the output is periodic with the same period as the input signal [23], the output can be described by the Fourier series [24]

$$u_r(t) = \sum_{n=1}^{\infty} |H_n(\omega)|\hat{e}_r\sin\left(n(\omega t + \varphi_{e_r}) + \angle H_n(\omega)\right) \tag{7}$$

where H_1 is called the SIDF and all H_n with $n > 1$ are referred to as the HOSIDFs, $n \in \mathbb{N}$. A quasi-linear approximation of a reset controller, equivalent to a Bode plot of an LTI system, can be created by means of the SIDF [25]. However, (7) shows that reset control systems suffer from the effect of harmonic generation. This denotes that the output signal, given an input sinusoid of a certain frequency, consists of not only the excitation frequency but also higher order harmonics at multiples of the excitation frequency [26]. The HOSIDFs introduced in [24] provide information on the generation of the higher order harmonics. The HOSIDFs for reset controller $\mathcal{R}$ with the reset condition as in (3) can be analytically computed using [10, Th. 3.1] (see also [27]), which is for convenience repeated in Theorem 1.

Theorem 1 [10, Th. 3.1]: For a reset controller $\mathcal{R}$ as in (1) with reset condition (3), the HOSIDFs are given by

$$H_n(\omega) = \begin{cases} C_r(j\omega I - A_r)^{-1}\left(I + j\Theta_D(\omega)\right)B_r + D_r, & \text{for } n = 1 \\ C_r(j\omega n I - A_r)^{-1} j\Theta_D(\omega)B_r, & \text{for odd } n \geq 2 \\ 0, & \text{for even } n \geq 2 \end{cases} \tag{8}$$

with $j := \sqrt{-1}$ and

$$\begin{aligned} \Lambda(\omega) &= \omega^2 I + A_r^2 \\ \Delta(\omega) &= I + e^{\frac{\pi}{\omega}A_r} \\ \Delta_r(\omega) &= I + A_\rho e^{\frac{\pi}{\omega}A_r} \\ \Gamma_r(\omega) &= \Delta_r^{-1}(\omega)A_\rho\Delta(\omega)\Lambda^{-1}(\omega) \\ \Theta_D(\omega) &= \frac{-2\omega^2}{\pi}\Delta(\omega)\left[\Gamma_r(\omega) - \Lambda^{-1}(\omega)\right]. \end{aligned}$$

The HOSIDFs can be easily augmented in case LTI systems are present in series before or after the reset controller, as depicted in Fig. 1. The resulting open-loop steady-state output signal given an input sinusoid (4) can be computed as an infinite sum of sinusoids

$$u(t) = \sum_{n=1}^{\infty} |C_1(j\omega)||H_n(\omega)||C_2(nj\omega)|\hat{e}\sin\big(n(\omega t + \varphi_e) + n\angle C_1(j\omega) + \angle H_n(\omega) + \angle C_2(nj\omega)\big). \tag{9}$$

The effectiveness of loopshaping in case of LTI systems comes from the fact that the open loop and closed loop can be easily related through the sensitivity equations. However, Saikumar et al. [10] showed that HOSIDFs are usually not negligible in closed loop, even when having a low magnitude, and simply utilizing the SIDF provides a highly inaccurate approximation of the closed-loop FRF. In [28, Definition 5], the so-called pseudo-sensitivity $S_\infty(\omega)$ was proposed, with magnitude defined as

$$|S_\infty(\omega)| = \frac{\max_{0<t<2\pi/\omega} e_{ss}(\omega, t)}{r_0} \tag{10}$$

where $e_{ss}(\omega, t)$ is the steady-state error of the closed-loop reset system excited by a reference input $r(t) = r_0\sin(\omega t)$, with $r_0 \in \mathbb{R}^+$. The pseudo-sensitivity allows to combine the information on closed-loop higher order harmonics into an analog of a sensitivity function for reset systems, thus helpful for loopshaping. Although the principle of superposition does not hold, the pseudo-sensitivity functions can still provide a reliable quantitative steady-state performance prediction to effectively design reset controllers for nonsinusoidal inputs, as shown in [29]. An analytical method that is able to relate open- and closed-loop HOSIDFs, based on a nonparametric plant model (FRF) given some assumptions, was established in [10] and is given in Theorem 2.

Theorem 2 [10]: Given a closed-loop reset system with input $r = \sin(\omega t)$, the steady-state error is given by

$$e_{ss}(t) = \sum_{n=1}^{\infty} |S_n(j\omega)| \sin\left(n\omega t + \angle S_n(j\omega)\right) \tag{11}$$

with

$$S_n(j\omega) = \begin{cases} S_1(j\omega), & \text{for } n = 1 \\ -\dfrac{L_n(j\omega)}{1 + L_{\text{BLS}}(nj\omega)}\left(|S_1(j\omega)|e^{jn\angle S_1(j\omega)}\right), & \text{for odd } n \geq 2 \\ 0, & \text{for even } n \geq 2 \end{cases} \tag{12}$$

and

$$S_1(j\omega) = \frac{1}{1 + L_1(j\omega)}$$
$$L_n(j\omega) = G(jn\omega)C_2(jn\omega)H_n(\omega)C_1(j\omega)e^{j(n-1)\angle C_1(j\omega)}$$

as long as the following assumptions hold true.

1) The system is input-to-state convergent.
2) The resets are a result of only the first harmonic of e_r.

The first assumption of Theorem 2, on input-to-state convergence, holds when the reset system satisfies the H_β-condition [28]. The second assumption allows the signal e_r to be nonsinusoidal, as long as the zero crossings of the first harmonic and the actual signal coincide. When the controller is designed such that the higher order harmonics of e_r are kept small compared to the first harmonic, this second assumption shows to be useful. Namely, the accuracy of closed-loop steady-state performance prediction can be improved compared to the SIDF method, as shown in [10].

Remark 1: In Theorem 2, the effect of measurement noise is not considered, although it can potentially have an effect on the reset instants. In this work, we assume that the effect of measurement noise on error e is negligible. However, this does not necessarily mean that measurement noise is negligible in signal e_r, which is further discussed in Section III.

D. Practical Aspects When Tuning With HOSIDFs

HOSIDFs are the prevailing method to perform steady-state performance prediction for reset systems in the frequency domain. Nevertheless, some aspects must be considered when utilizing this method. First, in this work, the control design is done in such a manner that the magnitude of all higher order harmonics is low compared to the first harmonic such that they do not have a major impact on the response. Namely, in that case, the closed-loop steady-state performance can be accurately predicted using Theorem 2. If the higher order harmonics are not small, it is unclear what the steady-state performance of the system looks like. Furthermore, given that the first harmonic is dominant, the SIDF can still be a useful aid in the control design procedure.

Theorem 1 allows to compute open-loop HOSIDFs only for reset controllers with continuous dynamics for the BLS. In case of a discrete implementation of the base linear dynamics, we will therefore assume that the sampling frequency is high enough to assure that the change in the HOSIDFs caused by discretization is negligible in the frequency range of interest.

As shown in (11), the greater the number of HOSIDFs that are accounted for in the sum, the more accurate the result. However, as for the open-loop method, when using a plant FRF, which is the common practical industry standard, information on the nth HOSIDF can be provided only for frequencies $\omega \leq \omega_{\max}/n$, where $\omega_{\max} \in \mathbb{R}^+$ is the largest frequency for which FRF data is available. This makes the accuracy of the method frequency dependent: the higher the frequency, the less HOSIDFs can be taken into account, and hence, the more inaccurate the result. Nevertheless, this still provides more information and thus a more accurate solution than solely using the SIDF to compute the closed-loop HOSIDFs. In fact, the method was utilized in [10] for design of the controller for a precision positioning stage.

A pseudo-sensitivity can be viewed as a "worst case scenario" closed-loop sensitivity in terms of steady-state performance, as only information on the maximum amplitude is regarded. This conservative approach ensures that the reset controller does not excessively amplify signals of certain frequencies in the closed loop. A constraint on the peak of the pseudo-sensitivity is not equivalent to robustness, but it prevents large amplification of the reference profile.

III. PCI-PID

A PCI is a resetting integrator with corner frequency $\omega_r \in \mathbb{R}^+$. The state-space matrices of a PCI are given by

$$A_r = 0, \quad B_r = \omega_r, \quad C_r = 1, \quad D_r = 1, \quad A_\rho = \gamma. \tag{13}$$

The nonlinearity affects mostly the low frequencies in the range $\omega < \omega_r$, where the resetting leads to a smaller phase lag compared to a linear integrator and a constant positive offset in magnitude. Nevertheless, contrary to a PI, a PCI cannot be utilized to suppress steady-state errors. This is due to the fact that resetting causes the stored energy from the integral action, required to avoid a steady-state error, to be eliminated, introducing a limit-cycle behavior [30]. Therefore, instead of replacing the "PI-part" of the linear PID controller with a PCI element, the PCI element can be utilized in addition to the existing linear PID.

Industrial motion stages are commonly controlled by cutting-edge feedforward controllers, which are capable of tracking a predetermined reference. Feedback control is then needed mostly to increase tracking precision by suppressing disturbances or to compensate for the dynamics not modeled in the feedforward controller. For improved tracking precision, increasing the open-loop gain at low frequencies is necessary. Due to Bode's gain–phase relationship, increasing this gain affects the phase margin of the system and thus its stability and robustness. With reset control, this limitation can be overcome, allowing a larger low-frequency open-loop gain compared to an LTI system for the same phase margin, according to the SIDF. However, note that a PCI also introduces phase lag, be it in a reduced extent compared to a PI. Therefore, a system controlled by a PCI-PID controller has an increased magnitude peak in the pseudo-sensitivity compared to the same system

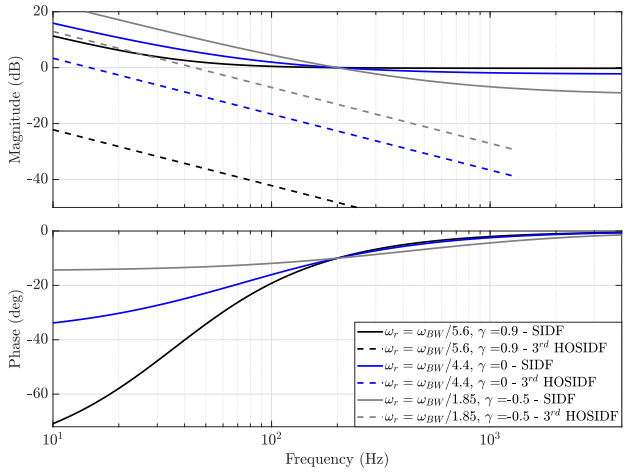

Fig. 2. Magnitude and phase characteristics of the SIDF and 3rd harmonic of three PCI elements with different combinations of ω_r and γ resulting in a phase lag of 10° at 200 Hz. The gain was adjusted to keep the crossover frequency ω_{BW} at 200 Hz.

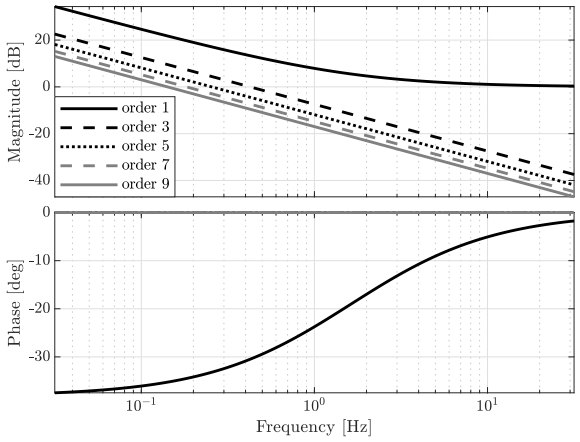

Fig. 3. Magnitude and phase characteristics of the odd-order HOSIDFs of a PCI as in (1), (3), and (13), with $\omega_r = 2\pi$ and $\gamma = 0$.

controlled solely by the same PID controller. This magnitude increase must be accounted for, by assuring that the PCI is used with an LTI controller with a high phase margin. A PCI-PID is then constructed by selecting $C_1 = 1$, $\mathcal{R}$ as a PCI and C_2 as an LTI PID controller, defined as

$$C_{\mathrm{PID}}(s) = \underbrace{k_P}_{P}\ \underbrace{\left(1+\frac{\omega_I}{s}\right)}_{I}\ \underbrace{\left(\left(1+\frac{s}{\omega_D}\right)\Big/\left(1+\frac{s}{\omega_T}\right)\right)}_{D} \tag{14}$$

with $k_P \in \mathbb{R}$ and ω_I, ω_D, $\omega_T \in \mathbb{R}^+$ in rad/s.

As a PCI only has two parameters, ω_r and γ, its tuning is relatively straightforward. By increasing ω_r, the magnitude and phase behavior of the SIDF and HOSIDFs can be shifted to the right. This increase will lead to a higher gain at frequencies lower than the bandwidth but also larger magnitude for the HOSIDFs and a lower phase margin. A similar effect is given by γ. A decreasing γ leads to a smaller phase lag and slightly greater gain at the cost of larger magnitude for the HOSIDFs. As depicted in Fig. 2, the same phase margin can thus be achieved for different combinations of γ and ω_r. Note that the magnitudes of the PCI's HOSIDFs with $n > 3$ have a similar shape as that of the 3rd HOSIDF but with a lower gain, as portrayed in Fig. 3. For this reason, only analyzing the 3rd HOSIDF is usually sufficient in order to comprehend the behavior of all HOSIDFs [10].

A. Lowering HOSIDFs

The tradeoff between HOSIDFs and low-frequency gain poses a constraint on the tuning of a PCI element. Therefore, lowering the HOSIDFs without affecting the SIDF would be beneficial, which can be achieved by using the CR architecture developed in [20]. The principle can be explained from (9). The magnitude of the nth HOSIDF is directly proportional to $|C_1(j\omega)|$ and $|C_2(jn\omega)|$. Therefore, to minimize the HOSIDFs, a lead element should be placed in C_1 and a lag element in C_2. An n_lth-order lead filter F_l can be defined as

$$F_l(s) = \left(\frac{\frac{s}{\omega_d}+1}{\frac{s}{\omega_t}+1}\right)^{n_l}, \quad \omega_d < \omega_t \tag{15}$$

with ω_d, $\omega_t \in \mathbb{R}^+$ in rad/s and $n_l \in \mathbb{N}$. When the PID is kept in C_2, but F_l and F_l^{-1} are added to C_1 and C_2, respectively, tuning the magnitude of HOSIDFs and their active region is possible without affecting the SIDF. Furthermore, when stability is assessed by means of the H_β-condition [31], filters F_l and F_l^{-1} have no influence on the analysis. To determine the range in which HOSIDFs have the most significant effect and which HOSIDF has the greatest effect, the power spectral density of the error signal when utilizing a PCI-PID without CR can be analyzed. In case feedforward control is employed, most of the power is usually caused by either external disturbances or resonances not modeled in the feedforward. If a disturbance/resonance is present at frequency ω_{dis}, the nth HOSIDF will show undesired excitation of higher order harmonics at frequency $n\omega_{\mathrm{dis}}$. By choosing $\omega_d = \omega_{\mathrm{dis}}$ and $\omega_t = n\omega_{\mathrm{dis}}$, the relative suppression of the nth HOSIDF at $\omega = \omega_{\mathrm{dis}}$ caused by adding the CR elements can be defined as $H_\varsigma(\omega_{\mathrm{dis}}, n) = |F_l(j\omega_{\mathrm{dis}})||F_l^{-1}(jn\omega_{\mathrm{dis}})|$. The lead filter order n_l can then be increased such that the amount of suppression is also increased by a factor $n_l H_\varsigma(\omega_{\mathrm{dis}}, n)$.

B. Effect of Noise

As shown in [20], having C_1 as a first-order lead filter results in the reset instants being affected not only by e but also by $\dot{e}$. The change in reset instants will affect steady-state performance in case noise is present in the system. To compute the open-loop SIDF and HOSIDFs, Theorem 1 assumes that the input is a sinusoid, which allows to predetermine the reset instants t_k. When noise is present in the system, the reset instants could differ. With a greater power of the noise, there is a higher chance for one of these undesired resets. A lead element such as F_l increases the magnitude of the high-frequency content of the output signal. The power of the noise present in the error signal e at ω is therefore increased with increasing $H_\varsigma(\omega_{\mathrm{dis}}, n)$, hence causing the SIDF and HOSIDFs to be more unreliable.

Next, the effect of noise on the CR architecture will be visualized through an example. A PCI-PID was tuned for a plant resembling a highly damped noncollocated double

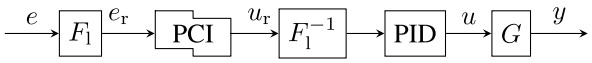

Fig. 4. Series CR PCI-PID block diagram.

TABLE I
PARAMETER VALUES OF G_1, PID_1, PCI, AND F_l, USED FOR CR_1 AND CR_2

G_1	m_1	m_2	k	d
	100	100	1.97×10^9	4.6×10^4
PID_1	k_P	ω_I	ω_D	ω_T
	8.204×10^7	20 Hz	76.92 Hz	520 Hz
PCI	ω_r	γ		
	60 Hz	0		
CR_1	ω_d	ω_t	n_l	
	50 Hz	50×3 Hz	1	
CR_2	ω_d	ω_t	n_l	
	50 Hz	50×3 Hz	2	

mass-spring-damper system

$$G_1(s) = \frac{ds + k}{m_1 m_2 s^4 + d(m_1 + m_2)s^3 + k(m_1 + m_2)s^2} \quad (16)$$

with parameter values given in Table I. The parameter values of the respective LTI PID controller PID_1 and the PCI are also given in the table. The open-loop block diagram is pictured in Fig. 4. PID_1 was tuned such that the LTI part of the open-loop system has $\approx 40°$ phase margin at $\omega_{\text{BW}} = 200$ Hz, allowing the PCI to have 10° phase lag at 200 Hz for the open-loop SIDF phase margin to be 30°. Two different F_l and F_l^{-1} pairs were tuned allowing to utilize two CR architectures, CR_1 and CR_2, respectively, with the corresponding parameter values also given in Table I. Both F_l and F_l^{-1} pairs have the same ω_d and ω_t, while $n_l = 1$ for CR_1 and $n_l = 2$ for CR_2, and both pairs are tuned assuming a disturbance $d = \sin(\omega_{\text{dis}} t)$, where $\omega_{\text{dis}} = 50$ Hz, which is acting on the system. Thus, through the tuning, we assure that $H_\varsigma(\omega_{\text{dis}}, 3) < 0$ dB. In fact, for CR_1, $H_\varsigma(\omega_{\text{dis}}, 3) = -6.02$ dB, and for CR_2, $H_\varsigma(\omega_{\text{dis}}, 3) = -12.04$ dB. The resulting open-loop FRFs are visualized in Fig. 5. The figure shows that the HOSIDFs are lowered with increasing $H_\varsigma(\omega_{\text{dis}}, n)$, whereas the SIDF remains unchanged. The magnitude plots of the pseudo-sensitivities are given in Fig. 6, which have been computed using Theorem 2 after discretizing all LTI parts of the system at 8 kHz using Tustin's approximation. As expected, a decrease in $H_\varsigma(\omega_{\text{dis}}, n)$ at low frequencies corresponds to a lower magnitude of the pseudo-sensitivity. Hence, better disturbance suppression can be achieved, caused by the suppression of the HOSIDFs.

A Simulink simulation was then performed with inputs $r(t) = 0$, $n(t) = 0$, and $d(t) = \sin(\omega_{\text{dis}} t)$, where $\omega_{\text{dis}} = 50$ Hz. The resulting closed-loop errors are given in Fig. 7. The cumulative power spectral density (CPSD) of the PCI-PID system without CR shows that the power spectrum has peaks at odd multiples of ω_{dis}, such as 150 and 250 Hz. These power peaks are the peaks of the third and the fifth harmonics resulting from the 50-Hz disturbance frequency. The improvement in performance resulting from the lower HOSIDFs at ω_{dis} introduced by the CR architecture is clearly to be seen. While the peak at 50 Hz in the CPSD remains almost identical, showing that the SIDF does not change, the peaks at 150 and 250 Hz decrease with decreasing $H_\varsigma(\omega_{\text{dis}}, n)$. The simulation shown in Fig. 7 is repeated with n being white noise in Fig. 8. The figure shows that an increase in $H_\varsigma(\omega_{\text{dis}}, n)$ still results in lower excitation of higher order harmonics; however, in this case, the three signals have a different suppression of the disturbance frequency itself, confirming that the SIDF is less reliable in the presence of noise.

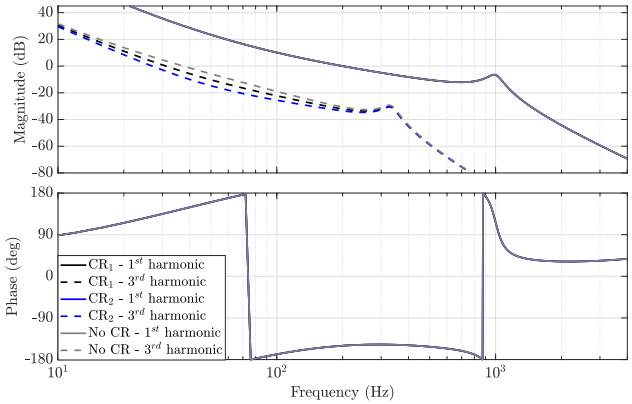

Fig. 5. Magnitude and phase characteristics of the SIDF and 3rd harmonic of the open-loop system with G_1 as the plant, PID_1 as the PID controller, and PCI as $\mathcal{R}$ and without CR architecture, with CR_1 or CR_2, respectively. All SIDFs are identical and therefore plotted on top of each other.

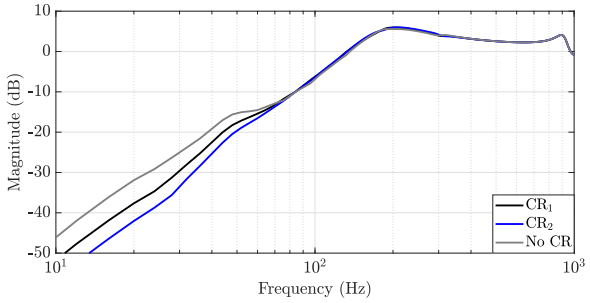

Fig. 6. Pseudo-sensitivity magnitudes computed through the approximate method (Theorem 2) of the closed-loop system with G_1 as the plant, PID_1 as the PID controller, and PCI as $\mathcal{R}$ and without CR architecture, with CR_1 or CR_2, discretized at 8 kHz.

IV. PARALLEL CR PCI-PID

With the CR architecture, HOSIDFs can be successfully reduced in a certain frequency range, without affecting the SIDF. Nevertheless, the architecture suffers from limitations, caused by the effect of amplifying the high-frequent power content in the error signal through F_l. To avoid this, a novel parallel CR architecture is proposed. The block diagram of the structure is depicted in Fig. 9. In order to make use of the performance analysis methods presented in Section II, the parallel CR architecture must be able to be represented using (1). A reset system $\mathcal{R}$ in parallel with C_{par}, as given in Fig. 9, can be described by an augmented reset system $\mathcal{R}$ given by

$$\begin{aligned} A_r &= \begin{bmatrix} \hat{A}_r & 0 \\ 0 & A_{C_{\text{par}}} \end{bmatrix}, \quad B_r = \begin{bmatrix} \hat{B}_r \\ B_{C_{\text{par}}} \end{bmatrix} \\ C_r &= \begin{bmatrix} \hat{C}_r & C_{C_{\text{par}}} \end{bmatrix}, \quad D_r = \begin{bmatrix} \hat{D}_r + D_{C_{\text{par}}} \end{bmatrix} \\ A_\rho &= \begin{bmatrix} \hat{A}_\rho & 0 \\ 0 & I^{n_{C_{\text{par}}} \times n_{C_{\text{par}}}} \end{bmatrix}, \quad C_1 = 1 \end{aligned} \quad (17)$$

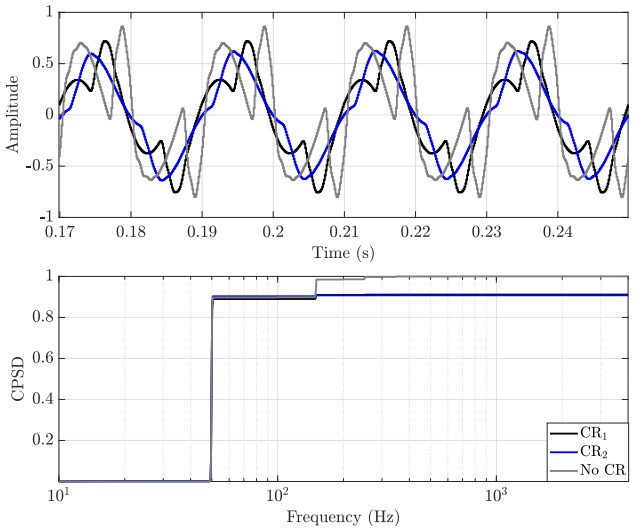

Fig. 7. Normalized closed-loop steady-state error signal (only four periods shown) resulting from a Simulink simulation of a system with G_1 as the plant, PID_1 as the PID controller, and PCI as $\mathcal{R}$ and without CR architecture, with CR_1 or with CR_2. The inputs to the system are $r(t) = 0$, $n(t) = 0$, and $d(t) = \sin(\omega_{\text{dis}} t)$, where $\omega_{\text{dis}} = 50$ Hz.

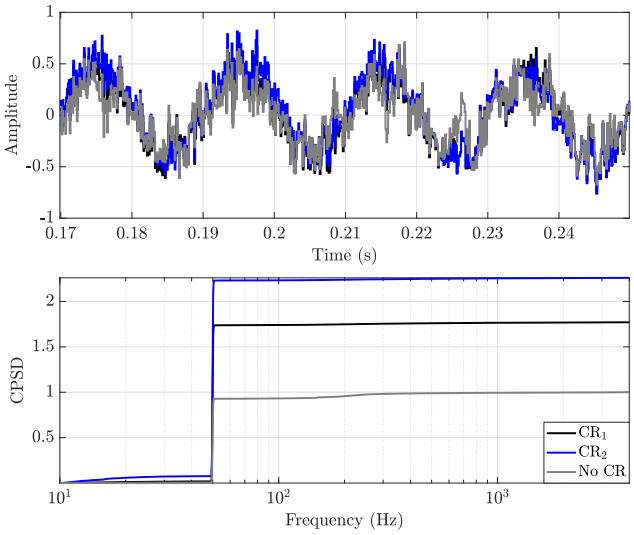

Fig. 8. Normalized closed-loop steady-state error signal (only four periods shown) resulting from a Simulink simulation of a system with G_1 as the plant, PID_1 as the PID controller, and PCI as $\mathcal{R}$ and without CR architecture, with CR_1 or CR_2. The inputs to the system are $r(t) = 0$, $n(t)$ is white noise with power 1×10^{-5} m^2 Hz^{-1}, and $d(t) = \sin(\omega_{\text{dis}} t)$, where $\omega_{\text{dis}} = 50$ Hz.

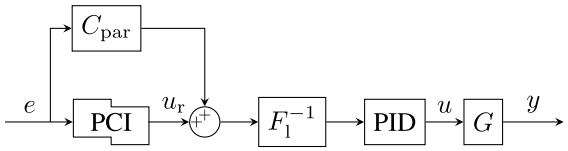

Fig. 9. Parallel CR PCI-PID block diagram.

with $\hat{A}_r, \hat{B}_r, \hat{C}_r, \hat{D}_r$, and $\hat{A}_\rho$ the state-space matrices of the resetting part of $\mathcal{R}$ (e.g., a PCI) and $n_{C_{\text{par}}} \in \mathbb{Z}^+$ the number of states of C_{par}. Using this definition, all theorems presented in Section II hold.

For a fully LTI system (i.e., $\mathcal{R} = R$), one can observe that the parallel CR architecture is equivalent to the series CR architecture when choosing $C_{\text{par}}(s) = R(s)\big(F_l(s) - 1\big)$. However, when resetting is introduced, this is no longer true.

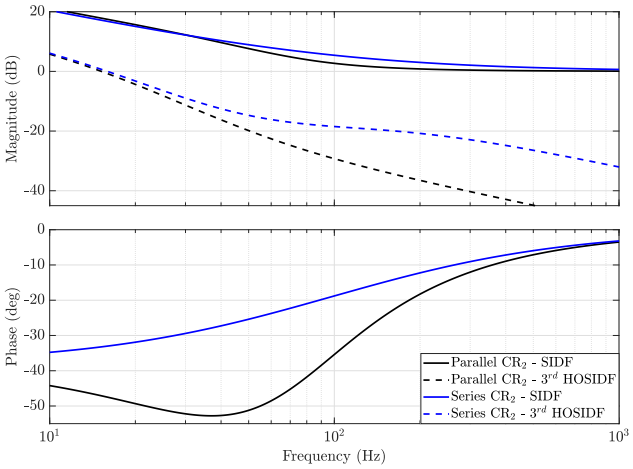

Fig. 10. Magnitude and phase characteristics of the SIDF and 3rd harmonic of the PCI in the series CR_2 architecture and a parallel CR_2 architecture with $\text{PI}_{\text{par}} = R$, without the PID and plant.

Therefore, in case $\mathcal{R}$ is a PCI, an approximation with

$$C_{\text{par}}(s) = \text{PI}_{\text{par}}(s)\big(F_l(s) - 1\big),\ \text{PI}_{\text{par}}(s) = 1 + \frac{\omega_{i_{\text{par}}}}{s} \quad (18)$$

can be utilized instead. When $\mathcal{R} \neq R$, the open-loop SIDF is not identical to the equivalent system without CR, contrary to the conventional series CR architecture. This is confirmed in Fig. 10, where the PCI in series with CR_2 is compared to a parallel CR architecture with the same parameters, thus with $\omega_{i_{\text{par}}} = \omega_r$. For low frequencies, the parallel CR structure approximates the series structure: for $\lim_{\omega \to 0} |C_{\text{par}}| = ((2\omega_{i_{\text{par}}}(\omega_t - \omega_d))/\omega_d \omega_t)$, which is negligible compared to $\lim_{\omega \to 0} |\text{PCI}| = \infty$. For high frequencies, the magnitude of the parallel architecture approaches $\frac{\omega_t^2 - \omega_d^2}{\omega_t^2}$. Namely, $\lim_{\omega \to \infty} |F_l^{-1}| = \left(\frac{\omega_d}{\omega_t}\right)^2$, and $\lim_{\omega \to \infty} |C_{\text{par}}| = \frac{\omega_t^2 - \omega_d^2}{\omega_d^2}$, which is dominant over $\lim_{\omega \to \infty} |\text{PCI}| = 1$. For low ω_d, this is a good approximation for the series architecture, which instead approaches 1. However, in the mid-frequency range, the parallel architecture has a smaller gain and lower phase. Furthermore, the HOSIDFs are also different between the two structures, with the parallel architecture having significantly lower HOSIDFs in the frequency range $\omega > \omega_d$. This is due to the fact that in a series CR architecture, the magnitude of the HOSIDFs depends on $|C_1(j\omega)|$, whereas in a parallel CR architecture, it is not dependent on $|C_{\text{par}}(j\omega)|$. In fact, control element C_{par} only contributes to the first harmonic, as illustrated in Fig. 11. For a parallel CR system such as the one shown in Fig. 9, with $C_2 = F_l^{-1}\text{PID}$, (9) becomes

$$\begin{aligned} u(t) = {} & |C_{\text{par}}(j\omega)||C_2(j\omega)|\hat{e} \sin\big(\omega t + \varphi_e + \angle C_{\text{par}}(j\omega) \\ & + \angle C_2(j\omega)\big) + \sum_{n=1}^{\infty} |H_n(\omega)||C_2(jn\omega)|\hat{e} \sin\big(n(\omega t + \varphi_e) \\ & + \angle H_n(\omega) + \angle C_2(jn\omega)\big). \end{aligned} \quad (19)$$

Since the HOSIDFs in the parallel CR architecture are significantly lower than the series CR architecture in the range $\omega > \omega_d$, this allows for γ to be lowered while still maintaining lower HOSIDFs in the range of interest compared to a PCI-PID without CR. The effect of γ on the parallel CR

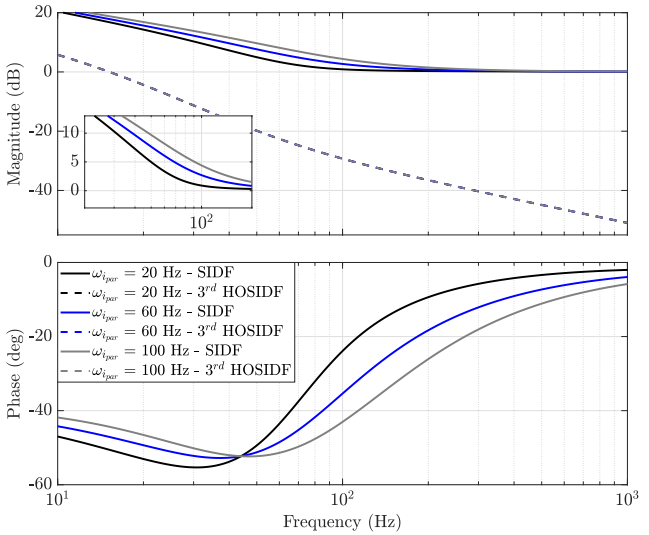

Fig. 11. Magnitude and phase characteristics of the SIDF and 3rd harmonic of the PCI in the parallel CR_2 architecture for different values of $\omega_{i_{\text{par}}}$ without PID or a plant. All 3rd harmonics are identical and therefore plotted on top of each other.

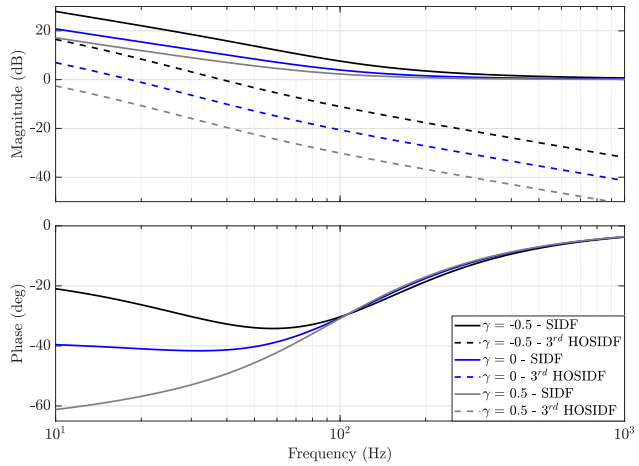

Fig. 12. Magnitude and phase characteristics of the SIDF and 3rd harmonic of the PCI in the parallel CR_2 architecture for different values of γ, without PID or a plant.

architecture is portrayed in Fig. 12. The HOSIDFs increase over the entire frequency range, while the SIDF increases in the low- and mid-frequency ranges. The proposed tuning procedure for a parallel CR PCI-PID is thus as follows.

Tuning Procedure (Parallel CR PCI-PID): The procedure is given as follows.

1) Tune a series CR PCI-PID first according to [20]. Initially choose $n_l = 1$.
2) Choose $\omega_{i_{\text{par}}} = \omega_r$ as an initial guess and compute C_{par} using (18).
3) Transform the series CR PCI-PID into a parallel CR PCI-PID, by setting $C_1 = 1$ and adding C_{par} in parallel of $\mathcal{R}$.
4) Lower γ until the difference between the SIDF and the HOSIDFs (in dB) over the entire frequency range of interest (i.e., where expected disturbances are located) is the same or greater than with the series CR architecture.
5) Lower $\omega_{i_{\text{par}}}$ until the phase at ω_{BW} is the same as with the series CR architecture.

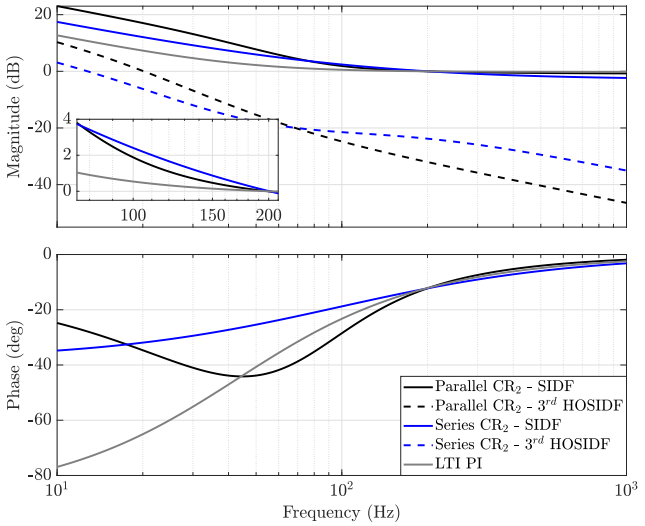

Fig. 13. Magnitude and phase characteristics of the SIDF and the 3rd harmonic of the PCI in the series CR_2 architecture, a parallel CR_2 architecture with $\omega_{i_{\text{par}}} = 30$ Hz and $\gamma = -0.3$, as well as an LTI PI element with equivalent phase lag at 200 Hz.

6) Adjust gain k_P to set the crossover frequency at ω_{BW}.
7) In case the peak of the pseudo-sensitivity magnitude must be decreased further (i.e., it is higher than the acceptable level, e.g., 6 dB), return to step 5, however aiming at obtaining a higher phase at ω_{BW}.
8) In case the peak of the pseudo-sensitivity magnitude can be increased further (i.e., it is lower than the acceptable level, e.g., 6 dB), return to step 5, however aiming at obtaining a lower phase at ω_{BW}.
9) Increase n_l and repeat steps 2–8. Choose the controller whose pseudo-sensitivity results in the lowest gain at the desired frequency range.

The tuning procedure was performed to convert the series CR_2 PCI-PID controller into a parallel CR controller. The gain was adjusted to keep the 200-Hz crossover frequency such that $\omega_{i_{\text{par}}} = 30$ Hz and $\gamma = -0.3$ were found. The controller's SIDF and HOSIDFs are depicted in Fig. 13 where an LTI PI controller with the same phase at the crossover frequency as the two CR PCI controllers is also shown. For the same phase margin and a greater difference between the first and third harmonics in the range $\omega > 50$ Hz, the parallel CR PCI-PID achieves a greater SIDF gain in the low-frequency range. However, in the range [70, 200] Hz, the series CR architecture provides a slightly greater gain. Nevertheless, compared to the LTI system, the parallel CR system still has a larger gain. Furthermore, at higher frequencies, the series CR PCI has a slightly lower SIDF and thus provides better noise and disturbance suppression.

V. Practical Implementation of a Reset Controller

So far, we assumed that the reset controller acts in the continuous time domain. However, in reality, a discrete-time reset controller is implemented in the physical system. In order to describe the dynamics of a discrete-time reset controller, (1)

(a) (b)

Fig. 14. (a) ASMPT wire bonder whose motion stage was utilized in this work. (b) Isolated XYZ-motion platform of the wire bonder.

was modified to

$$\tilde{\mathcal{R}} = \begin{cases} x_{r,k+1} = \tilde{A}_r x_{r,k} + \tilde{B}_r e_{r,k}, & \text{if } (e_{r,k}, e_{r,k-1}) \notin \tilde{\mathcal{M}} \\ x_{r,k+1} = \tilde{A}_r A_\rho x_{r,k} + \tilde{B}_r e_{r,k}, & \text{if } (e_{r,k}, e_{r,k-1}) \in \tilde{\mathcal{M}} \\ u_{r,k} = \tilde{C}_r x_{r,k} + \tilde{D}_r e_{r,k}, & \text{if } (e_{r,k}, e_{r,k-1}) \notin \tilde{\mathcal{M}} \\ u_{r,k} = \tilde{C}_r A_\rho x_{r,k} + \tilde{D}_r e_{r,k}, & \text{if } (e_{r,k}, e_{r,k-1}) \in \tilde{\mathcal{M}} \end{cases} \tag{20}$$

with

$$\tilde{\mathcal{M}} := \{e_{r,k} e_{r,k-1} \leq 0\} \tag{21}$$

where $\tilde{A}_r$, $\tilde{B}_r$, $\tilde{C}_r$, and $\tilde{D}_r$ are the state-space matrices of the discretized BLS and $k \in \mathbb{N}$ is the sample index. Resetting is based on the condition that e_r in the current sample changes sign compared to the previous sample, as in (21). Therefore, the sampling time imposes a time-regularization constraint, as in-between samples no resetting can occur. The condition is beneficial as it avoids the occurrence of Zenoness, a cause of ill-posedness, defined as the presence of infinite reset actions in a finite time [32].

VI. Experimental Setup and Results

A. Experimental Setup

The isolated motion stage of a wirebonding machine [Fig. 14(a) and (b)] is utilized to experimentally validate the results obtained in this work. The wire bonder's motion platform is subdivided into an X-, a Y-, and a Z-stage, allowing the end-effector to translate in three degrees of freedom. The positions of the three stages are measured by high-resolution optical encoders, resulting in low measurement noise levels compared with the error signals. The motion platform is designed and calibrated in such a manner that each motion axis can be assumed to be SISO LTI within its operating regime. In this work, only the X-stage is utilized, which represents the plant G in Fig. 1. The nonparametric plant model of the X-stage is given in Fig. 15, which shows the identified FRF from the actuator current that is applied to the X-stage to its measured encoder position. The FRF from the actuator of the Y-stage to the X-stage encoder position is

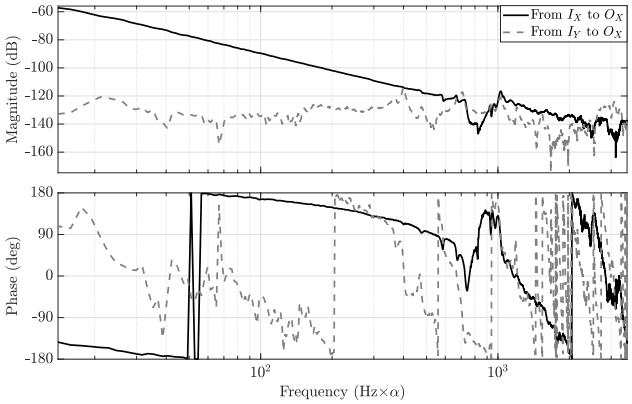

Fig. 15. Identified FRF between X- (I_X) and Y-stages (I_Y) actuator current and X-stage encoder position (O_X) at the center position.

also portrayed in the figure, which shows that the influence of cross couplings can be neglected until beyond the aimed control bandwidth frequency. One can also observe that the system suffers from a transport delay, which limits the control system's bandwidth [33]. Due to confidentiality, the frequency axis in the figure has been scaled by an arbitrary constant α.

Currently, SISO LTI feedback and feedforward control is employed to regulate the motion of each of the three stages. The feedforward controller makes sure that the errors during motions are reduced to acceptable levels. However, the base frame that connects the stage to the ground is excited during motion, which results in undesired low-frequent disturbance forces that are acting on the system even after the motion has finished. The resulting positioning error has to be compensated by means of feedback control. After the end of motion, high-precision wirebonding processes have to take place. By reducing the positioning error, these processes can start faster and wirebonding becomes more accurate. Therefore, improving the feedback controller is crucial for the system's overall performance.

B. Experimental Results

An LTI PI-PID controller was tuned first using the tuning procedure from [34], which requires first selecting a bandwidth frequency ω_{BW} based on the plant's resonances and phase lag, as seen from its FRF (Fig. 15), and then assigning the PID parameters given in (14) based on rules of thumb. A PI was then added, which decreased the phase margin. This was recompensated by increasing the D-action, thus slightly decreasing ω_D and slightly increasing ω_T. A notch filter was also added to suppress the plant's resonance. The PID parameters were adjusted until a high bandwidth and a peak of sensitivity of 6 dB were assured. The PI was then converted into a PCI. Subsequently, the PCI's integrator frequency ω_I could be increased due to the lower phase lag, thus allowing to increase the low-frequency gain without affecting the peak of sensitivity. A series CR PCI-PID was tuned next following the tuning procedure in [20]. This series structure was then converted to a parallel CR PCI-PID using the tuning procedure in Section IV. The controllers' parameter values are not revealed due to confidentiality. The scaled open-loop FRF plots are portrayed in Fig. 16, whereas the respective

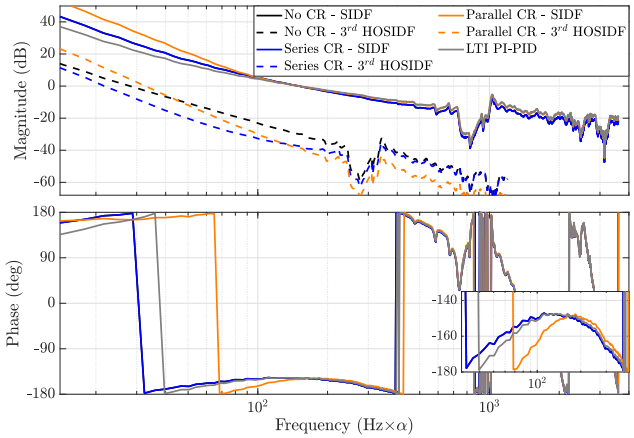

Fig. 16. Magnitude and phase characteristics of the SIDF and 3rd harmonic of the open-loop system with the wire bonder's X-stage (at the center position) as the plant and different reset control structures. The SIDFs of the series CR and No CR PCI-PID are identical and therefore plotted on top of each other.

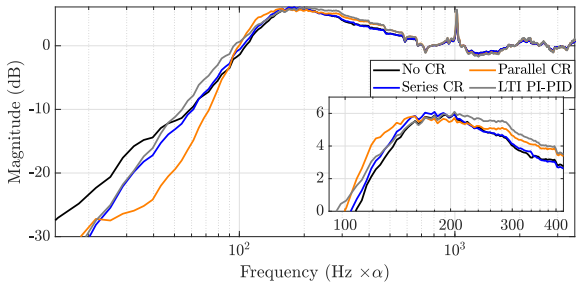

Fig. 17. Magnitude characteristics of the pseudo-sensitivities for the closed-loop system (Fig. 1) with the wire bonder's X-stage (at the center position) as the plant and different reset control structures.

magnitude plots of the pseudo-sensitivities, computed through the approximate method, are plotted in Fig. 17. The figures show that all reset systems have greater open-loop gain at low frequencies compared to the LTI system, for the same magnitude-peak of the pseudo-sensitivity. Moreover, as expected, the parallel CR system has a larger open-loop magnitude compared to the respective series CR systems with the same F_l. However, for the case without CR, the larger open-loop gain—compared to the LTI system—does not translate into a lower magnitude of the pseudo-sensitivitiy in a part of the low-frequency range. This undesired behavior is caused by the excitation of higher order harmonics, and, as expected, is reduced significantly by utilizing the series CR architecture. By utilizing the parallel CR system, the magnitude of the pseudo-sensitivity can be lowered even further compared to the series CR architecture. Nevertheless, in a certain range before ω_{BW}, the magnitude of pseudo-sensitivities of the system controlled by the parallel CR PCI-PID is higher compared to the system controlled by the respective series CR PCI-PID. This behavior is related to the tradeoff of the magnitude of parallel CR architecture in the mid-frequency range already mentioned in Section IV.

The scaled resulting error signals, for a typical reference trajectory, are portrayed in Fig. 18. The reference trajectory consists of a smooth forward and backward move from 0 to $r_{\max}$ and from $r_{\max}$ back to 0, which primarily contains energy below the control bandwidth frequency. Fig. 18 also shows the CPSDs of the error signal in the phase after the motion has

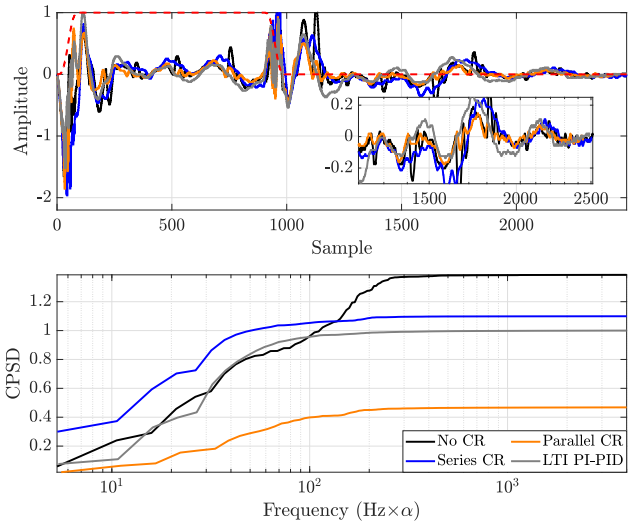

Fig. 18. Normalized error signals and CPSDs of the steady-state phase obtained from experiments for a typical reference trajectory (the reference is scaled).

TABLE II
NORMALIZED e_{rms} OBTAINED IN EXPERIMENTS WITH DIFFERENT CONTROLLER STRUCTURES

	No CR	series CR	parallel CR	LTI
e_{RMS}	1.1763	1.0491	0.6839	1

ended. This phase is defined as the period between sample $k_{\mathrm{set}} \in \mathbb{N}$, the sample at which the reference signal reaches 0 after the backward move and the final sample. The root mean square (rms) of the error after the end of motion is defined as

$$e_{\mathrm{rms}} = \sqrt{\frac{1}{1+k_n-k_{\mathrm{set}}}\left(\sum_{k=k_{\mathrm{set}}}^{k_n} e_k^2\right)} \tag{22}$$

where $k_n \in \mathbb{N}$ is the total number of samples. This metric is a good indicator for the accuracy of the wirebonding process. The resulting rms errors, normalized with respect to the e_{rms} resulting from the LTI PI-PID system, are given in Table II. The PCI-PID system without CR has a greater e_{rms} than the fully LTI system due to the prevalence of HOSIDFs. The excitation of higher order harmonics is accounted for partially using the series CR architecture, which shows significantly lower power in the higher frequencies. However, at the same time, the series CR structure results in increased power at the first harmonic. This shows that the noise present in the system is amplified by this architecture to the point where performance deteriorates. Finally, the highest suppression of the first harmonic is achieved by the parallel CR structure. The parallel CR architecture reduces the rms error by 32% compared to the LTI system.

Remark 2: The feedback control output that is generated by reset controllers can in some cases be significantly larger than for an LTI controller [20], which can potentially lead to actuator saturation. However, note that for the application considered in this work, the feedforward controller takes up the majority of the control output. Therefore, the control effort that is desired by the reset controller is not an issue.

VII. Conclusion

In this work, a novel parallel CR architecture is developed. Furthermore, tuning guidelines for a parallel CR PCI-PID controller, based on loopshaping, are presented. These guidelines are obtained by employing open- and closed-loop HOSIDFs as a frequency-domain-based steady-state performance prediction tool. The parallel CR architecture allows to overcome a practical limitation of the existing series CR architecture: high-frequency noise amplification. This benefit is achieved by avoiding using a lead filter before the reset element as in the series CR architecture, which causes amplification of the high-frequent power content in the error signal.

The findings are validated through experiments, consisting of tracking a typical reference signal on a wirebonding machine, in the presence of both feedforward and feedback control. The PCI-PID system without CR architecture shows how the system's main disturbance is suppressed more effectively compared to a PI-PID system with the same bandwidth and peak of (pseudo)sensitivity. However, excitation of higher order harmonics of the disturbance frequency led to a significant decrease in performance. The series CR PCI-PID demonstrated its effectiveness at lowering the excitation of higher order harmonics. However, the series CR structure shows an overall worse performance compared to the LTI PI-PID system, evidencing that when tuned inappropriately the noise can cause significant performance degradation in systems employing the series CR architecture. The parallel CR architecture achieves the best performance, with a 32% reduction in the rms error after the end of motion when compared to the LTI PI-PID controller. Although this work highlights the potential of the parallel CR architecture, we should note that this solution is designed specifically for the wirebonding machine and might not be generally applicable. For example, this method is only applicable if the frequency of the problematic vibration in the error signal is significantly smaller than the sampling frequency.

We have several recommendations for further research. First, existing stability analysis tools that apply to parallel CR systems, such as the classical H_β-condition, still require a parametric plant description. Recently, the so-called Nyquist stability vector (NSV) [11] method has been proposed for some types of reset systems that are similar to the ones containing a parallel CR architecture. This method is equivalent to the H_β-condition but also allows to use a nonparametric plant description (FRF). A recommendation for future work is thus to augment the NSV method to include the parallel CR architecture. In fact, an augmented NSV method for a reset element with a similar structure as (17) was already presented in [11]. Second, a further limitation in the design of reset controllers is given by the assumptions required to use the approximate method to compute pseudo-sensitivities (Theorem 2). Especially, when HOSIDFs are high, the method can result in inaccurate results. For this reason, improving the current method in future works would be beneficial. Finally, studying the transient performance of the proposed control architecture in more detail is of particular interest.

References

[1] S. B. Joseph, E. G. Dada, A. Abidemi, D. O. Oyewola, and B. M. Khammas, "Metaheuristic algorithms for PID controller parameters tuning: Review, approaches and open problems," *Heliyon*, vol. 8, no. 5, May 2022, Art. no. e09399.

[2] K. Åström and R. Murray, *Feedback Systems: An Introduction for Scientists and Engineers*. Princeton, NJ, USA: Princeton Univ. Press, 2010.

[3] H. W. Bode, *Network Analysis and Feedback Amplifier Design*. New York, NY, USA: Van Nostrand, 1945.

[4] S. Skogestad and I. Postlethwaite, *Multivariable Feedback Control: Analysis and Design*. Hoboken, NJ, USA: Wiley, 2005.

[5] D. van Dinther et al., "Overcoming performance limitations of linear control with hybrid integrator-gain systems," *IFAC-PapersOnLine*, vol. 54, no. 5, pp. 289–294, 2021.

[6] G. Zhao, D. Nešić, Y. Tan, and C. Hua, "Overcoming overshoot performance limitations of linear systems with reset control," *Automatica*, vol. 101, pp. 27–35, Mar. 2019.

[7] B. G. B. Hunnekens, N. van de Wouw, and D. Nešić, "Overcoming a fundamental time-domain performance limitation by nonlinear control," *Automatica*, vol. 67, pp. 277–281, May 2016.

[8] K. J. Åström and T. Hägglund, "The future of PID control," *Control Eng. Pract.*, vol. 9, no. 11, pp. 1163–1175, 2001.

[9] M. Heertjes and M. Steinbuch, "Stability and performance of a variable gain controller with application to a dvd storage drive," *Automatica*, vol. 40, no. 4, pp. 591–602, Apr. 2004.

[10] N. Saikumar, K. Heinen, and S. H. HosseinNia, "Loop-shaping for reset control systems: A higher-order sinusoidal-input describing functions approach," *Control Eng. Pract.*, vol. 111, Jun. 2021, Art. no. 104808.

[11] A. A. Dastjerdi, "Frequency-domain analysis of 'constant in gain lead in phase (CGLP)' reset compensators," Ph.D. dissertation, Dept. Precis. Microsystems Eng., Delft Univ. Technology, Delft, The Netherlands, 2021.

[12] L. F. van Eijk, S. Beer, R. M. J. van Es, D. Kostic, and H. Nijmeijer, "Frequency-domain properties of the hybrid integrator-gain system and its application as a nonlinear lag filter," *IEEE Trans. Control Syst. Technol.*, vol. 31, no. 2, pp. 905–912, Mar. 2023.

[13] V. Utkin and A. Poznyak, "Adaptive sliding mode control," in *Advances in Sliding Mode Control*. Berlin, Germany: Springer, 2013.

[14] J. C. Clegg, "A nonlinear integrator for servomechanisms," *Trans. Amer. Inst. Elect. Eng., II, Appl. Ind.*, vol. 77, no. 1, pp. 41–42, 1958.

[15] Y. Chait and C. V. Hollot, "On Horowitz's contributions to reset control," *Int. J. Robust Nonlinear Control*, vol. 12, no. 4, pp. 335–355, 2002.

[16] N. Saikumar, R. K. Sinha, and S. H. HosseinNia, "'Constant in gain lead in phase' element–application in precision motion control," *IEEE/ASME Trans. Mechatronics*, vol. 24, no. 3, pp. 1176–1185, Jun. 2019.

[17] N. Karbasizadeh, N. Saikumar, and S. Hossein Nia Kani, "Fractional-order single state reset element," *Nonlinear Dyn.*, vol. 104, no. 1, pp. 413–427, 2021.

[18] N. Karbasizadeh, A. A. Dastjerdi, N. Saikumar, and S. H. HosseinNia, "Band-passing nonlinearity in reset elements," *IEEE Trans. Control Syst. Technol.*, vol. 31, no. 1, pp. 333–343, Jan. 2023.

[19] E. Akyüz, N. Saikumar, and S. H. HosseinNia, "Reset control for vibration disturbance rejection," *IFAC-PapersOnLine*, vol. 52, no. 15, pp. 525–530, 2019.

[20] N. Karbasizadeh and S. H. HosseinNia, "Continuous reset element: Transient and steady-state analysis for precision motion systems," *Control Eng. Pract.*, vol. 126, Sep. 2022, Art. no. 105232.

[21] L. Zaccarian, D. Nesic, and A. Teel, "First order reset elements and the Clegg integrator revisited," in *Proc. Amer. Control Conf.*, vol. 1, Jun. 2005, pp. 563–568.

[22] J. A. G. Prieto, A. Barreiro, and S. Dormido, "Frequency domain properties of reset systems with multiple reset anticipations," *IET Control Theory Appl.*, vol. 7, no. 6, pp. 796–809, 2013.

[23] Y. Guo, Y. Wang, and L. Xie, "Frequency-domain properties of reset systems with application in hard-disk-drive systems," *IEEE Trans. Control Syst. Technol.*, vol. 17, no. 6, pp. 1446–1453, Nov. 2009.

[24] P. Nuij, O. Bosgra, and M. Steinbuch, "Higher-order sinusoidal input describing functions for the analysis of non-linear systems with harmonic responses," *Mech. Syst. Signal Process.*, vol. 20, no. 8, pp. 1883–1904, 2006.

[25] M. Vidyasagar, *Nonlinear Systems Analysis*, 2nd ed. Upper Saddle River, NJ, USA: Prentice-Hall, 1993.

[26] D. Rijlaarsdam, P. Nuij, J. Schoukens, and M. Steinbuch, "A comparative overview of frequency domain methods for nonlinear systems," *Mechatronics*, vol. 42, pp. 11–24, Apr. 2017.
[27] N. Saikumar, K. Heinen, and S. H. HosseinNia, "Corrigendum to 'Loop-shaping for reset control systems: A higher-order sinusoidal-input describing functions approach' [Control Engineering Practice 111 (2021) 104808]," *Control Eng. Pract.*, vol. 137, Jun. 2023, Art. no. 105565.
[28] A. A. Dastjerdi, A. Astolfi, N. Saikumar, N. Karbasizadeh, D. Valério, and S. H. HosseinNia, "Closed-loop frequency analysis of reset control systems," *IEEE Trans. Autom. Control*, vol. 68, no. 2, pp. 1146–1153, Feb. 2023.
[29] A. A. Dastjerdi, N. Saikumar, and S. H. HosseinNia, "Tuning of a class of reset elements using pseudo-sensitivities," in *Proc. Eur. Control Conf. (ECC)*, Jun. 2021, pp. 1187–1192.
[30] A. Barreiro, A. Baños, S. Dormido, and J. A. González-Prieto, "Reset control systems with reset band: Well-posedness, limit cycles and stability analysis," *Syst. Control Lett.*, vol. 63, pp. 1–11, Jan. 2014.
[31] O. Beker, "Analysis of reset control systems," Ph.D. dissertation, Dept. Elect. Comput. Eng., Univ. Massachusetts Amherst, Amherst, MA, USA, 2001.
[32] A. Baños and A. Barreiro, *Reset Control Systems*, vol. 9. London, U.K.: Springer, Oct. 2012.
[33] L. van Eijk, "Nonlinear motion control designs and performance evaluation on an industrial motion stage," M.S. thesis, Dept. Mech. Eng., Eindhoven Univ. Technol., Eindhoven, The Netherlands, 2021.
[34] R. Munnig Schmidt, G. Schitter, and J. van Eijk, *The Design of High Performance Mechatronics. High-Tech Functionality by Multidisciplinary System Integration*. Amsterdam, The Netherlands: IOS Press, 2011.

Daniel Caporale received the M.Sc. degree (cum laude) in mechanical engineering with specialization in mechatronics from Delft University of Technology, Delft, The Netherlands, in 2022.

He is currently working as a Mechatronics Engineer at ASML, Veldhoven, The Netherlands.

Luke F. van Eijk received the B.Sc. (cum laude) and M.Sc. (Hons.) degrees in mechanical engineering from Eindhoven University of Technology, Eindhoven, The Netherlands, in 2018 and 2021, with a focus on dynamics and control. He is currently pursuing the Ph.D. degree within the Department of Precision and Microsystems Engineering, Delft University of Technology, Delft, The Netherlands.

He is working as a Mechatronics Engineer at ASMPT, Beuningen, The Netherlands. His research interests are in the analysis and design of (non)linear feedback controllers, with a particular focus on reset control and the hybrid integrator-gain system.

Nima Karbasizadeh (Member, IEEE) received the M.Sc. degree in mechatronics engineering from the University of Tehran, Tehran, Iran, in 2017, and the Ph.D. degree in mechatronic system design from Delft University of Technology, Delft, The Netherlands, in 2023, with a focus on reset and complex-order control.

In 2023, he joined ASML, Veldhoven, The Netherlands, where he has been working as a Mechatronics Engineer focusing on high-precision mechatronics for semiconductor manufacturing. His research interests include precision motion control, nonlinear precision control, reset control, complex-order control, and mechatronic system design.

Stijn Beer received the B.Sc. degree in mechanical engineering and the M.Sc. degree in systems and control from Eindhoven University of Technology, Eindhoven, The Netherlands, in 2017 and 2019, respectively.

He started his professional career at ASMPT, Beuningen, The Netherlands, as a Mechatronics Engineer. He is currently working at ASML, Veldhoven, The Netherlands, as an Integration Engineer for the wafer handler of lithography systems. His research interests include system identification, modeling of dynamical systems, and data-based and nonlinear motion controller design.

Dragan Kostić received the Ph.D. degree in control technology and robotics from Eindhoven University of Technology, Eindhoven, The Netherlands, in 2004.

He works at ASMPT, Beuningen, The Netherlands, as the Research and Development Director for mechatronics. His professional positions range from research and teaching at knowledge institutions to professional engineering in commercial companies. Multidisciplinary system modeling and identification, data-based controls, and nonlinear control designs are his main areas of expertise. His current research interests include modeling, dynamical analysis, and control of hi-tech mechatronic systems for semiconductor manufacturing.

S. Hassan HosseinNia (Senior Member, IEEE) received the Ph.D. degree (Hons. and cum laude) in electrical engineering specializing in automatic control: application in mechatronics from the University of Extremadura, Badajoz, Spain, in 2013.

Since October 2014, he has been appointed as a Faculty Member at the Department of Precision and Microsystems Engineering, Delft University of Technology, Delft, The Netherlands. He has an industrial background, having worked at ABB, västerås, Sweden. He has (co-)authored over 150 publications in respected journals, conference proceedings, and book chapters. His main research interests include precision mechatronic system design, precision motion control, and mechatronic systems with distributed actuation and sensing.

Dr. HosseinNia served as the General Chair for the 7th IEEE International Conference on Control, Mechatronics, and Automation (ICCMA 2019). Currently, he is an Editorial Board Member of the following journals: *Fractional Calculus and Applied Analysis*, *Frontiers in Control Engineering*, and *International Journal of Advanced Robotic Systems* (SAGE).